Electrocatalysis

Deutsche Ausgabe: DOI: 10.1002/ange.201601367
Internationale Ausgabe: DOI: 10.1002/anie.201601367

Cobalt-Nanocrystal-Assembled Hollow Nanoparticles for Electrocatalytic Hydrogen Generation from Neutral-pH Water

*Bingrui Liu, Lin Zhang, Weilin Xiong, and Mingming Ma**

Abstract: *Highly active and stable electrocatalysts for hydrogen generation from neutral-pH water are highly desired, but very difficult to achieve. Herein we report a facile synthetic approach to cobalt nanocrystal assembled hollow nanoparticles (Co-HNP), which serve as an electrocatalyst for hydrogen generation from neutral-pH water. An electrode composed of Co-HNP on a carbon cloth (CC) produces cathodic current densities of 10 and 100 mA cm^{-2} at overpotentials of −85 mV and −237 mV, respectively. The Co-HNP/CC electrode retains its high activity after 20 h hydrogen generation at a high current density of 150 mA cm^{-2}, indicating the superior activity and stability of Co-HNP as electrocatalyst.*

Electrolysis of water, driven by electricity that is derived from renewable energy sources, could provide hydrogen as an ideal energy carrier for clean and sustainable energy technologies.[1] To achieve a high energy-conversion efficiency, active catalysts for the electrochemical hydrogen evolution reaction (HER) are required.[2] Employing a neutral-pH electrolyte solution prevents the use of undesirable strong acids or bases that could lead to environmental and handling issues. Nature's hydrogenase enzymes drive HER in neutral-pH solution with high efficiency and activity, but suffer from a low density of active sites and poor stability, which limit their practical use.[3] Noble metals, such as platinum, can facilitate HER effectively in a wide pH range, but their scarcity and high cost promotes the search for alternative HER catalysts based on earth-abundant elements.[4] A few non-noble metal compounds, such as CoS,[5] CoP,[6] FeP,[7] WP_2,[8] MoB,[9] Mo_2C,[9] MoS_x,[10] and H_2-CoCat,[11] have been investigated as catalysts with moderate activity for HER in neutral-pH solution. Some of them suffer from limited stability under operation conditions.[5,11] Therefore, highly active and stable electrocatalysts for HER in neutral-pH solution are highly desired, but remain very difficult to achieve.[5]

Owing to the high activity, good stability and tunability, noble-metal nanocrystals have abstracted intensive interests as active electrocatalysts for HER.[12] In contrast, there has been no report on non-noble metal nanocrystals as electrocatalysts for HER, most likely owing to the limited stability of non-noble metal nanocrystals. However, encapsulated by carbon nanoshells, iron metal nanoparticles have been reported with outstanding stability and catalytic activity for oxygen reduction reaction (ORR).[13] Cobalt metal nanocrystals (Co-NC) that are protected by surface oxides and borates can be facilely prepared by borohydride reduction methods,[14] which have been widely utilized as hydride-transfer catalysts for organic synthesis[15] and hydrogen generation by chemical reactions,[16] but have not been investigated as electrocatalysts for HER. Herein we report a facile synthetic approach to cobalt-nanocrystal-assembled hollow nanoparticles (Co-HNP), which serve as a highly active and stable electrocatalyst for HER from neutral-pH water. Tested in neutral-pH phosphate buffer, the electrode comprising Co-HNP on a carbon cloth (1.0 mg cm^{-2} mass loading) produced cathodic current densities of 10 and 100 mA cm^{-2} at overpotentials of −85 mV and −237 mV, respectively. The electrode activity was essentially unchanged after either 1000 cyclic voltammetric sweeps, or 20 h hydrogen generation at a high current density of 150 mA cm^{-2}.

Co-HNP was prepared using a "sacrificial template" method (Figure 1 a, see Supporting Information for details). Amorphous $CoWO_4$ nanoparticles (NPs) were prepared by a rapid precipitation reaction between $CoCl_2$ and Na_2WO_4 in water solution (Figure S1 in the Supporting Information, ca. 80 nm in diameter). Under an ultrasonication-assisted reduction reaction by sodium borohydride, CoB alloy deposited on the surface of $CoWO_4$ NPs and converted into protected Co-NC, while the amorphous $CoWO_4$ NPs dissolved to form a hollow structure. The extreme but transient local conditions caused by acoustic cavitation[17] could facilitate the uniform deposition of CoB alloy onto the surface of $CoWO_4$ NPs, the conversion from CoB alloy into Co-NC, and the fast dissolution of amorphous $CoWO_4$ NPs.[18] Thus, the wet-chemistry synthesis was done in 30 min under an ambient conditions, which is very convenient. Tungsten and phosphorous as doping elements were introduced to help to protect Co-NC and also improve the catalytic activity.[19] To optimize the catalytic performance of Co-HNP, we varied the synthetic parameters systematically and measured the catalytic activity of the Co-HNP products for HER, as shown in Figure S2 and S3. The most active Co-HNP catalyst was prepared with a reactant molar ratio of $CoCl_2$:Na_2WO_4 = 5:3, $NaBH_4$:NaH_2PO_2 = 3:2, and (Co + W):(B + P) = 1:4 (see Supporting Information for details).

Examined by scanning electron microscopy (SEM), the optimized Co-HNP appeared as nanoparticles with a diameter around 100 nm (Figure 1 b), with some broken ones showing the hollow structure. Transmission electron microscopy

[*] B. Liu, L. Zhang, W. Xiong, Prof. Dr. M. Ma
CAS Key Laboratory of Soft Matter Chemistry, iChEM (Collaborative Innovation Center of Chemistry for Energy Materials), Department of Chemistry, University of Science and Technology of China
Hefei, Anhui 230026 (P.R. China)
E-mail: mma@ustc.edu.cn
Homepage: http://staff.ustc.edu.cn/~mma/
Supporting information and the ORCID identification number(s) for the author(s) of this article can be found under http://dx.doi.org/10.1002/anie.201601367.

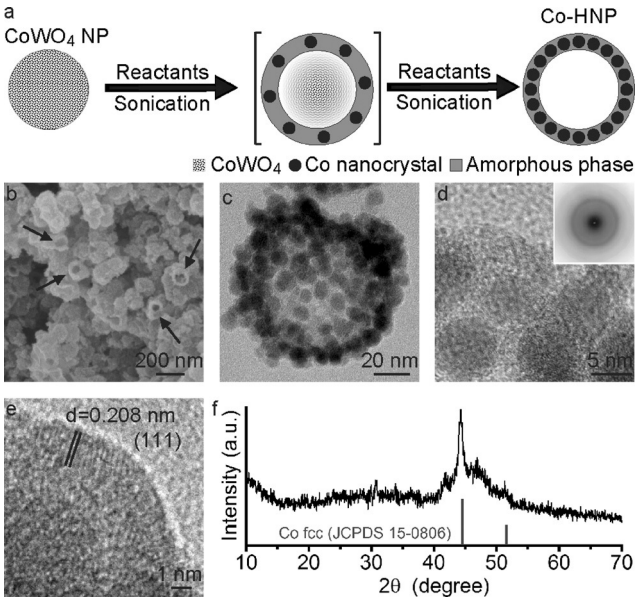

Figure 1. a) Schematic representation of the synthetic route Co-HNP. b) SEM and c) TEM images of Co-HNP, the black arrows indicate broken Co-HNP showing the hollow structure. d) HRTEM image showing the shell of Co-HNP is composed of nanocrystals and amorphous material. Inset: SAED pattern. e) HRTEM image of one nanocrystal showing the Co fcc phase. f) XRD patterns of Co-HNP, bars indicate the standard peaks of Co metal fcc phase (JCPDS 15-0806).

(TEM) image showed that the diameter of the inside cavity was around 80 nm (Figure 1c), consistent with the size of $CoWO_4$ NPs that served as sacrificial templates. The thin shell of each Co-HNP was composed by multiple 5–10 nm nanoparticles (the dark dots in Figure 1c). High-resolution TEM (HRTEM) image revealed the crystalline structure of these small nanoparticles (the dark particles in Figure 1d), which were surrounded by amorphous materials (the lighter region in Figure 1d). Selected area electron diffraction (SAED; Figure 1d inset) and HRTEM image (Figure 1e) identified these NC with an inter-plane spacing of 0.208 nm, corresponding to the (111) plane of cobalt face-centered cubic (fcc) phase. The two diffraction rings in SAED pattern recorded from these randomly oriented Co-NC can be assigned as the (111) and (110) planes of Co fcc phase, which was consistent with the powder X-ray diffraction (XRD) data (Figure 1f). By using Scherrer equation, the mean diameter of Co-NC was estimated based on the peak at $2\theta = 44°$ to be 5.5 nm, consistent with the observation by HRTEM (Figure 1d).

Elemental analysis of the optimized Co-HNP sample was performed by both X-ray photoelectron spectroscopy (XPS) (Figure S4) and energy dispersive X-ray spectroscopy (EDX) (Figure S5), which gave the atomic ratio Co:P:W:B = 9.7:1.3:1:6.6, indicating the majority element in Co-HNP was cobalt. XPS survey also provided valuable information of the chemical status of Co-HNP. In the Co 2p spectrum, two peaks at 776.9 eV and 791.7 eV were assigned to metallic cobalt, corresponding to the Co-NC, while the peaks at 780.2 eV and 796.1 eV with a broad shoulder at 785 eV indicated the existence of Co^{II} species, likely cobalt oxide.[14] The B 1s peak at 187.8 eV indicated B^0, while the stronger peak at 192.1 eV was attributed to borate species.[14] In the P 2p spectrum, the peak at 129.3 eV was attributed to P^0 or phosphide, while the bigger one locating at 133.8 eV was assigned to phosphate.[6a] The W 4f spectrum showed two sets of peaks at values of 31.4/34.2 eV and 35.8/38.0 eV, assigned to W^0 and W^{VI} species,[19] likely as W metal and tungstate, respectively. Thus, the XPS survey suggested the existence of cobalt oxide, boron oxide or borate, phosphate and tungstate on the surface of Co-HNP, consisting the amorphous layer to protect the Co-NC.[14] Raman spectrum of the Co-HNP sample (Figure S6) further confirms that the surface layer of Co-HNP is comprised of borate, CoO, phosphate and tungstate. On the other hand, the active site of HER reaction is like comprised by the low oxidation status elements. In fact, the peaks of elemental Co (776.9/791.7 eV), B (187.8 eV) and P (129.3 eV) of Co-HNP showed significant shifts from the standard values of elemental Co (778.2/793.4 eV), B (187.2 eV) and P (130.2 eV) (reference data from NIST Database, see Supporting Information and Figure S7 for details), which suggested a partial negative charge on Co and P atoms, and a partial positive charge on B atoms. Similar energy shifts have been reported for Co-B[20] and Co-P[6a] compounds as catalysts. Such shifts imply electron transfer among B, Co and P atoms, making Co and P electron-rich, and B electron-deficient, which likely comprise the catalytic active sites for HER. No shift was observed for W^0 and W^{VI} peaks, which implies a different role of W. Since W metal and alloys are highly resistant to oxidation, W^0 species in the Co-HNP could help to stabilize Co-HNP from oxidation, while W^{VI} species (likely tungstate) may act as Lewis acid sites to active water.[19]

Co-HNP was loaded on carbon cloth (CC) with a 1.0 mg cm^{-2} mass loading as the working electrode, through a facile drop-and-dry method without using any binder (see Supporting Information for details). Its catalytic activity for HER was tested in 1M pH 7 phosphate buffer at room temperature. Blank CC, cobalt metal plate and commercial Pt/C catalyst (20 wt% Pt on Vulcan XC-72) were also examined. As shown in Figure 2a, both blank CC and cobalt metal plate show negligible HER activity, while Pt/C shows superior HER activity with near-zero overpotential (η). Despite the low HER activity of bulk cobalt metal,[21] Co-HNP exhibits an excellent activity with a low onset η of 23 mV and a small Tafel slope value of 38 mV dec^{-1} (Figure 2b), which is superior to reported non-noble HER catalysts working in neutral-pH solution (Table S1). The Tafel slope of 38 mV dec^{-1} suggests that the catalytic process follows a Volmer–Heyrovsky mechanism.[22] The Co-HNP catalyst needs small η of 180 and 237 mV to drive current densities of 50 and 100 mA cm^{-2}, respectively. For comparison, an amorphous CoS film prepared via an electrodeposition method needs $\eta = 397$ mV to reach 50 mA cm^{-2}.[5] Another elegant example is CoP nanocrystals coating on CC, reaching current densities of 50 and 100 mA cm^{-2} at $\eta =$ 210 and 310 mV,[6a] which was the best one among previously reported non-noble-metal HER catalysts in neutral-pH solution (Table S1). The comparison with reported results demonstrates the superior activity of Co-HNP for HER in neutral-pH water.

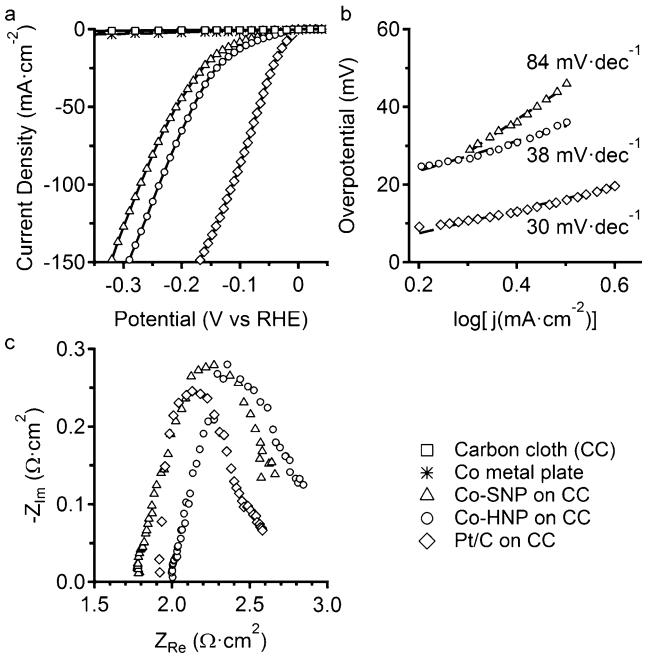

Figure 2. a) Polarization curves, b) Tafel plots and c) Nyquist plots of blank carbon cloth (CC), cobalt metal plate, Pt/C, Co-SNP, and Co-HNP. All catalysts were loaded on CC with the same loading (1.0 mg cm^{-2}) as working electrodes, which were tested in 1 M pH 7 phosphate buffer.

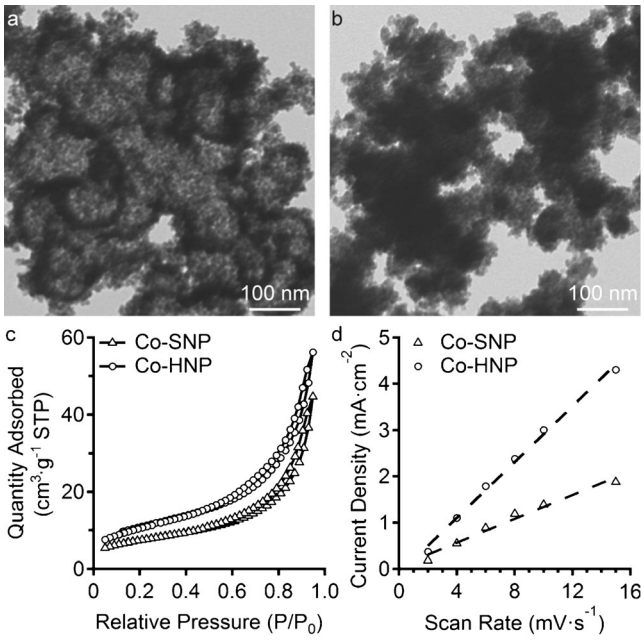

Figure 3. TEM images of a) Co-HNP (hollow) and b) Co-SNP (solid) showing different nanostructures assembled by Co-NC. c) Nitrogen adsorption/desorption isotherms and d) electrochemically active surface area measurements showing Co-HNP has a much larger specific surface area and active-site density than Co-SNP.

Well-designed nanostructures can enhance the catalytic activity, as a result of the increased specific surface area and quantum size effect.[23] To probe the effect of hollow nanostructures on the catalytic activity, Co-nanocrystal-assembled solid nanoparticles (Co-SNP) were prepared for side-by-side comparison with Co-HNP (see Supporting Information for the synthesis). Characterization of Co-SNP by XPS (Figure S8), XRD, SEM, and TEM (Figure S9) suggested that its chemical composition was very close to that of the Co-HNP. The size and phase of Co-NC in Co-SNP was also similar to that of the Co-HNP. The only one major difference between Co-SNP and Co-HNP was the solid versus hollow nanostructure. However, the catalytic performance of Co-HNP was clearly superior to that of Co-SNP (Figure 2a,b). Charge-transfer resistances (R_{ct}) were derived from electrochemical impedance spectroscopy (EIS; Figure 2c), which correlate to the intrinsic activity of electrocatalyst. Surprisingly, R_{ct} values of Pt/C (0.50 Ω cm^2), Co-HNP (0.56 Ω cm^2) and Co-SNP (0.58 Ω cm^2) were pretty close to each other, which implies the high intrinsic activity of Co-NC based catalysts. In addition, the ultrahigh electronic conductivity is one big advantage for metal nanocrystals over semi-conductive electrocatalysts, such as MoS_2, which displays large R_{ct} values, and often needs conductive support to form hybrid complex for sufficient charge transfer.[24] The close packaging of Co-NC ensures efficient charge transfer between active sites and the electrode substrate, which helps to achieve large current densities at low overpotentials.[25]

Since the Co-HNP and Co-SNP showed similar R_{ct} values, indicating similar intrinsic catalytic activity, the superior HER performance of the Co-HNP was attributed to the beneficial effect of a hollow nanostructure (Figure 3a) over solid one (Figure 3b).[25] The nitrogen adsorption/desorption isotherm (Figure 3c) of Co-HNP gave a Brunauer-Emmett-Teller (BET) surface area of 38 m^2 g^{-1}, while the BET surface area of Co-SNP was only 20 m^2 g^{-1}. Since a larger specific surface area may not correlate to larger catalytically active surface area, we measured the double-layer capacitance of electrodes by using cyclic voltammetry method, which serves as an estimate of the effective electrochemically active surface area.[26] The areal specific capacitances of Co-HNP and Co-SNP on CC electrode were calculated as 290 and 130 mF cm^{-2}, respectively (Figure 3d, Figure S10, see Supporting Information for details). The comparison demonstrates that the hollow nanostructure provides a larger catalytically active surface area than the solid nanostructure, because the hollow structure has more accessible active sites, located at both the interior and exterior surfaces of the nanoparticles.

The apparent exchange current density (j_0) of the Co-HNP/CC electrode was 1.53 mA cm^{-2}, calculated from the Tafel plot data in Figure 2b, which was two orders of magnitude higher that the j_0 value for Co metal (4.8 μA cm^{-2}).[21] The extremely large values of the areal specific capacitance and exchange current density of the Co-HNP/CC electrode can be explained by the large specific area of Co-HNP (38 m^2 g^{-1}), providing 380 cm^2 real surface area for 1.0 mg Co-HNP loading on 1 cm^2 carbon cloth. Divided by the factor of 380, the true exchange current density for Co-HNP was 4.0 μA cm^{-2}, which is close to the j_0 value for Co metal (4.8 μA cm^{-2}). Also, divided by the factor of 380, the true areal specific capacitance of Co-HNP was 0.76 mF cm^{-2}, which is comparable to the reported values of other crystal-

line catalysts for HER.[6a,25,27] Thus, it is the hollow nanostructure that greatly enhances the catalytic performance of Co-HNP/CC electrode.

For most of current HER electrocatalysts, the HER reaction at a high overpotential range is often severely affected by evolved hydrogen bubbles, which often stick to the hydrophobic surface of electrodes and limit the available active surface area and mass transport.[10,28] This issue can be partially solved by electrode rotation[28] or surface modification of electrodes.[29] Owing to the hydrophilic nature of oxides and borates on the surface of Co-HNP, the hydrophilic Co-HNP facilitates a quick release of hydrogen as tiny bubbles from the electrode surface, which can successfully suppress the interference from hydrogen bubbles. Thus, the Co-HNP/CC electrode can produce a high current density of 150 mA cm^{-2} at a relatively low overpotential of 290 mV (Figure 2a), without electrode rotation or stirring the solution, which is a highly desired property for the practical application of HER catalysts.

To probe the durability of the Co-HNP as electrocatalyst, continuous cyclic voltammetry (CV) was performed on Co-HNP electrode at a scanning rate of 50 mV s^{-1}. The polarization curve of Co-HNP/CC electrode after 1000 CV cycles overlays almost exactly with the initial one (Figure 4a), which

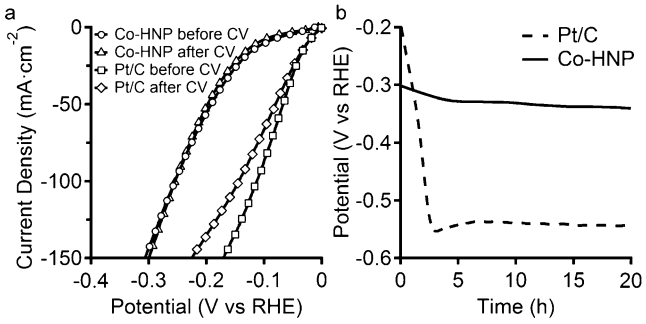

Figure 4. a) Polarization curves of Co-HNP or Pt/C electrodes before and after 1000 cyclic voltammetric sweeps. b) The overpotentials applied on Co-HNP or Pt/C electrodes during hydrogen generation at a static current density of 150 mA cm^{-2}. All the tests were performed in 1 M PBS buffer (pH 7).

suggests its good stability. In contrast, the polarization curve of Pt/C electrode after 1000 CV cycles shifts to the left, indicating a reduced activity. The practical operation of Co-HNP catalyst was examined by a long-term hydrogen generation experiment at a high current density of 150 mA cm^{-2}, and compared with the performance of Pt/C catalyst at the same condition (Figure 4b). For the Co-HNP electrode, a potential of −300 mV versus the reversible hydrogen electrode (RHE) was needed to drive the hydrogen generation. The potential gradually shifted to −330 mV in 5 h and remained there up to 20 h. XPS analysis of the post-HER Co-HNP sample shows no significant difference from the as-prepared Co-HNP sample (Figure S11). For the Pt/C electrode, a smaller potential of −190 mV was needed at the beginning, while the potential quickly shifted to −550 mV in 3 h and remained around −530 mV for the rest of time. The comparison clearly demonstrates the superior stability of Co-HNP over Pt/C as electrocatalyst at a heavy-loading operation condition in neutral-pH water.

In summary, we have developed a facile synthesis approach to prepare hollow nanostructures assembled by stabilized Co-NC. The optimized Co-HNP serves as an electrocatalyst for HER from neutral-pH water, which is able to drive a large cathodic current at low overpotentials, and offer stable operation at a heavy-loading over an extended period. To our knowledge, the Co-HNP is currently the most active and stable non-noble electrocatalyst for HER from neutral-pH water. Our results suggest that stabilized non-noble metal nanocrystals assembled in hollow nanostructures are promising subjects to study for developing highly active and stable electrocatalysts.

Acknowledgements

This work was supported by the National Natural Science Foundation of China (21474094) and the Recruitment Program of Global Experts.

Keywords: cobalt · electrocatalysis · hollow nanostructures · nanocrystals · water splitting

How to cite: *Angew. Chem. Int. Ed.* **2016**, *55*, 6725–6729
Angew. Chem. **2016**, *128*, 6837–6841

[1] a) J. Luo, J.-H. Im, M. T. Mayer, M. Schreier, M. K. Nazeeruddin, N.-G. Park, S. D. Tilley, H. J. Fan, M. Graetzel, *Science* **2014**, *345*, 1593–1596; b) H. B. Gray, *Nat. Chem.* **2009**, *1*, 7; c) T. R. Cook, D. K. Dogutan, S. Y. Reece, Y. Surendranath, T. S. Teets, D. G. Nocera, *Chem. Rev.* **2010**, *110*, 6474–6502.

[2] a) M. G. Walter, E. L. Warren, J. R. McKone, S. W. Boettcher, Q. Mi, E. A. Santori, N. S. Lewis, *Chem. Rev.* **2010**, *110*, 6446–6473; b) Y. Zhao, F. Zhao, X. P. Wang, C. Y. Xu, Z. P. Zhang, G. Q. Shi, L. T. Qu, *Angew. Chem. Int. Ed.* **2014**, *53*, 13934–13939; *Angew. Chem.* **2014**, *126*, 14154–14159.

[3] K. A. Vincent, A. Parkin, F. A. Armstrong, *Chem. Rev.* **2007**, *107*, 4366–4413.

[4] M. S. Faber, S. Jin, *Energy Environ. Sci.* **2014**, *7*, 3519–3542.

[5] Y. Sun, C. Liu, D. C. Grauer, J. Yano, J. R. Long, P. Yang, C. J. Chang, *J. Am. Chem. Soc.* **2013**, *135*, 17699–17702.

[6] a) J. Tian, Q. Liu, A. M. Asiri, X. Sun, *J. Am. Chem. Soc.* **2014**, *136*, 7587–7590; b) Z. Pu, Q. Liu, P. Jiang, A. M. Asiri, A. Y. Obaid, X. Sun, *Chem. Mater.* **2014**, *26*, 4326–4329.

[7] J. Tian, Q. Liu, Y. Liang, Z. Xing, A. M. Asiri, X. Sun, *ACS Appl. Mater. Interfaces* **2014**, *6*, 20579–20584.

[8] Z. Pu, Q. Liu, A. M. Asiri, X. Sun, *ACS Appl. Mater. Interfaces* **2014**, *6*, 21874–21879.

[9] H. Vrubel, X. Hu, *Angew. Chem. Int. Ed.* **2012**, *51*, 12703–12706; *Angew. Chem.* **2012**, *124*, 12875–12878.

[10] D. Merki, H. Vrubel, L. Rovelli, S. Fierro, X. Hu, *Chem. Sci.* **2012**, *3*, 2515–2525.

[11] S. Cobo, J. Heidkamp, P.-A. Jacques, J. Fize, V. Fourmond, L. Guetaz, B. Jousselme, V. Ivanova, H. Dau, S. Palacin, M. Fontecave, V. Artero, *Nat. Mater.* **2012**, *11*, 802–807.

[12] a) A. Chen, P. Holt-Hindle, *Chem. Rev.* **2010**, *110*, 3767–3804; b) S. Bai, C. Wang, M. Deng, M. Gong, Y. Bai, J. Jiang, Y. Xiong, *Angew. Chem. Int. Ed.* **2014**, *53*, 12120–12124; *Angew. Chem.* **2014**, *126*, 12316–12320.

[13] a) D. Deng, L. Yu, X. Chen, G. Wang, L. Jin, X. Pan, J. Deng, G. Sun, X. Bao, *Angew. Chem. Int. Ed.* **2013**, *52*, 371–375; *Angew.*

Chem. **2013**, *125*, 389 – 393; b) G. Wu, K. L. More, C. M. Johnston, P. Zelenay, *Science* **2011**, *332*, 443 – 447.
[14] G. M. Arzac, T. C. Rojas, A. Fernandez, *ChemCatChem* **2011**, *3*, 1305 – 1313.
[15] B. Ganem, J. O. Osby, *Chem. Rev.* **1986**, *86*, 763 – 780.
[16] S. S. Muir, X. Yao, *Int. J. Hydrogen Energy* **2011**, *36*, 5983 – 5997.
[17] N. A. Dhas, K. S. Suslick, *J. Am. Chem. Soc.* **2005**, *127*, 2368 – 2369.
[18] J. H. Bang, K. S. Suslick, *J. Am. Chem. Soc.* **2007**, *129*, 2242 – 2243.
[19] R. Fernandes, N. Patel, A. Miotello, R. Jaiswal, D. C. Kothari, *Int. J. Hydrogen Energy* **2012**, *37*, 2397 – 2406.
[20] H. X. Li, H. Li, M. H. Wang, *Appl. Catal. A* **2001**, *207*, 129 – 137.
[21] J. K. Nørskov, T. Bligaard, A. Logadottir, J. R. Kitchin, J. G. Chen, S. Pandelov, *J. Electrochem. Soc.* **2005**, *152*, J23 – J26.
[22] J. O. M. Bockris, E. C. Potter, *J. Electrochem. Soc.* **1952**, *99*, 169 – 186.
[23] a) C.-Y. Cao, Z.-M. Cui, C.-Q. Chen, W.-G. Song, W. Cai, *J. Phys. Chem. C* **2010**, *114*, 9865 – 9870; b) L. Wang, Y. Yamauchi, *J. Am. Chem. Soc.* **2013**, *135*, 16762 – 16765.
[24] Y. Li, H. Wang, L. Xie, Y. Liang, G. Hong, H. Dai, *J. Am. Chem. Soc.* **2011**, *133*, 7296 – 7299.
[25] M. S. Faber, R. Dziedzic, M. A. Lukowski, N. S. Kaiser, Q. Ding, S. Jin, *J. Am. Chem. Soc.* **2014**, *136*, 10053 – 10061.
[26] S. Trasatti, O. A. Petrii, *J. Electroanal. Chem.* **1992**, *327*, 353 – 376.
[27] D. Kong, H. Wang, Z. Lu, Y. Cui, *J. Am. Chem. Soc.* **2014**, *136*, 4897 – 4900.
[28] B. Cao, G. M. Veith, J. C. Neuefeind, R. R. Adzic, P. G. Khalifah, *J. Am. Chem. Soc.* **2013**, *135*, 19186 – 19192.
[29] Z. Lu, W. Zhu, X. Yu, H. Zhang, Y. Li, X. Sun, X. Wang, H. Wang, J. Wang, J. Luo, X. Lei, L. Jiang, *Adv. Mater.* **2014**, *26*, 2683 – 2687.

Received: February 6, 2016
Revised: March 9, 2016
Published online: April 29, 2016

